INVESTIGATION ON DONOR-ACCEPTOR PROPERTIES OF QUINIZARIN DYE WITH METAL OXIDES FOR DYE- SENSITIZED SOLAR CELL APPLICATIONS

S.Ranjitha[1], [1]Department of Physics, Velalar College of Engineering and Technology, Thindal, Erode- 638012, Tamil Nadu, India

S.Kalaiselvi[2] Department of Chemistry , Velalar College of Engineering and Technology, Thindal, Erode- 638012, Tamil Nadu, India

R.Padmavathi,[3] Department of Chemistry,M.Kumarasamy College of Engineering,Karur,Tamilnadu,India

S. Bhuvaneswari[4],Assistant Professor,Department of Physics,KPR Institute of Engineering and Technology,Coimbatore-641407

ABSTRACT

The investigation in optoelectronic parameters of the Quinizarin with semiconducting oxides at by (DFT/B3LYP) by employing a 6- 311G (d,p) basis are studies . The Electronic absorption spectrum was analyzed by TD-DFT methods and reported that wavelength is in the visible and near-UV regions. The oscillator strength; electrostatic potential confirms that was assigned to perform due to photo-induced electron transfer processes. Interaction between HOMO and LUMO of quinizarin with semiconducting oxides was explored to understand the recombination and charge transfer process involving with a bandgap of semiconductors. It shows that the effect on the process of electron injection, oxidation, and dye regeneration of DSSC applications. The photovoltaic characteristics study was performed to examine the role of charge transfer and the stability of the quinizarin dye molecule with semiconductor in the fabrication of DSSC compared with computational results.

Keywords: DSSC, Quinizarin, Current-Voltage characteristics, B3LYP

Corresponding Author:

ranjilotus21@gmail.com,09842903086

Introduction

The photovoltaics has emerged as a main source of energy due to its emphasis over the utilization of burning fossil fuels which has a harmful influence on the environment .The research on photovoltaics made its impact as an essential technology among the various

renewable sources of energy [1,2]. The development of photovoltaics is gaining attention and decreases environmental pollution and to live the mankind in a protected way. Solar cells based on single silicon crystals were the first generation devices that can evidence the highest photon to current conversion efficiency. The high production cost and installation of first-generation solar cells made various researchers to introduce the second generation solar cell devices made-up of semiconductor thin films. Due to the unavailability of efficient semiconductors, manufacturing costs and stability problems has led the path to the usage of organic dyes and pigments in the third generation solar cells popularly known as dye-sensitized solar cells (DSSCs). These devices are similar to plant photosynthesis that mechanizes the energy from the absorbed sunlight [3- 7] which is in the visible region. The work function of DSSC mainly depends on the quality of the materials, semiconductor electrode, and chemically synthesized photosensitizer with recombination with oxides. Even though several wide-bandgap metal oxide semiconductors are employed in the DSSCs, the TiO_2, ZnO, and ZrO_2 were the most predominantly and successfully used semiconductors. The sensitizer plays a significant role in absorbing light, nowadays, Ru (II) poly pyridyl complexes were reported to obtain the highest efficiency.But unfortunately, this material makes the solar cells expensive. This drawback leads to the development of low cost and high stability DSSCs with the use of organic dyes or natural dyes that were extracted from plants to explore their possibilities . However, metal-free organic dyes have been explored as an alternative to Ru-complexes because of low material costs, facile synthesis, and high molar extinction coefficients. The DSSCs based on metal-free organic dyes as sensitizers, with significantly good efficiencies have been reported [8,9], yet there is a necessity to optimize their Preparation of Dye-Sensitized Solar Cells

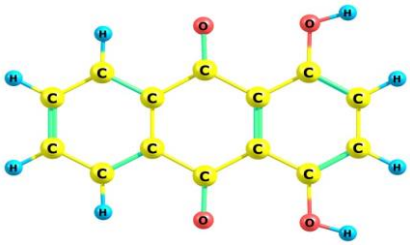

Quinizarin
(1,4-dihydroxyanthraquinone)

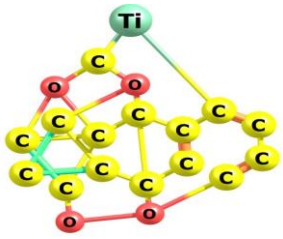

Quinizarin with TiO_2

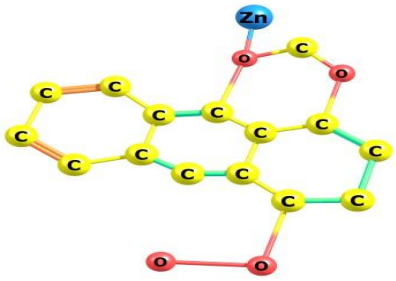

Quinizarin with ZnO

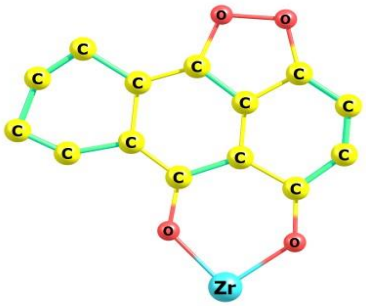

Quinizarin with ZrO_2

Figure 1 Optimized Geometrical Structure of Dye Quinizarin and Quinizarin with TiO_2, ZnO and ZrO_2

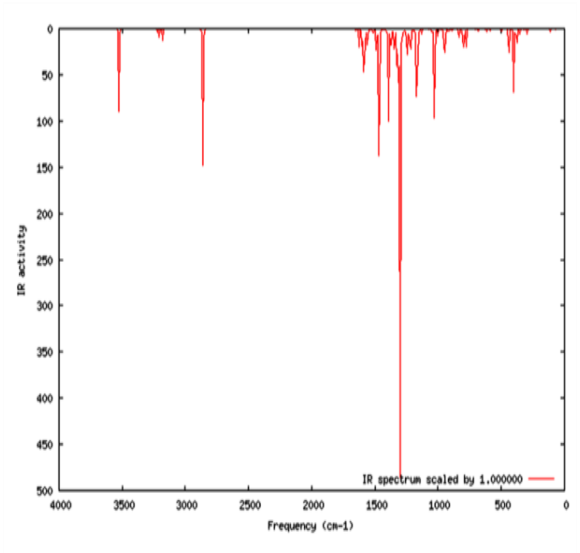

a)Quinizarin (1,4-dihydroxyanthraquinone)

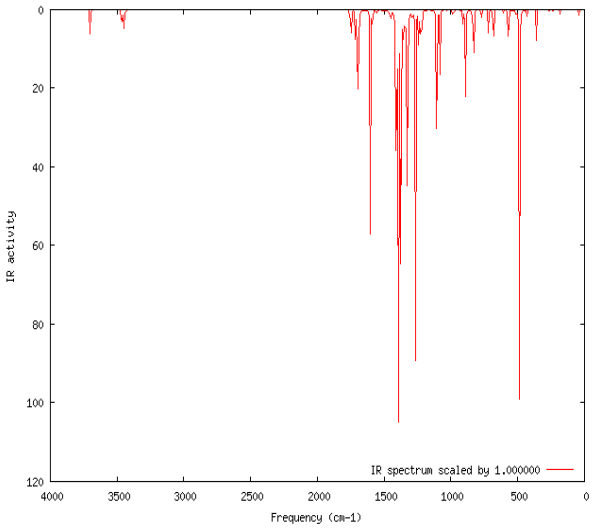

b) Quinizarin with TiO_2

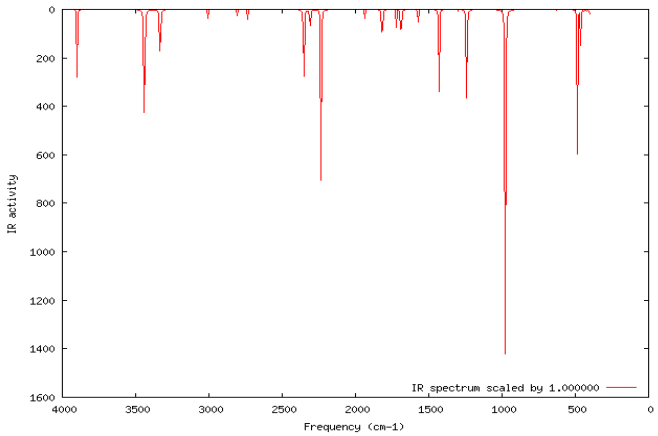

c) Quinizarin with ZnO

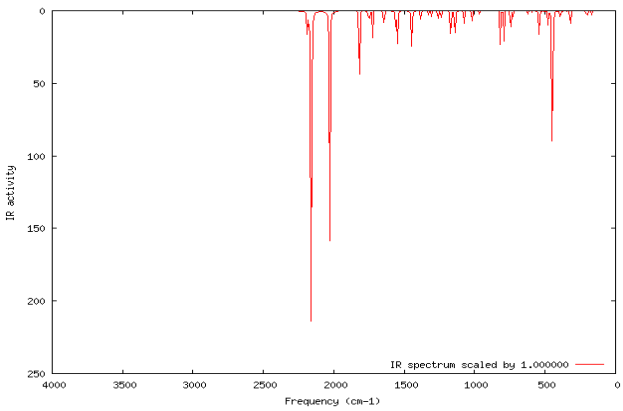

d) Quinizarin with ZrO_2

Figure 2(a,b,c,d) Theoretical Analysis of FT-IR Spectrum of Quinizarin and Quinizarin/TiO_2 ,ZnO and ZrO_2

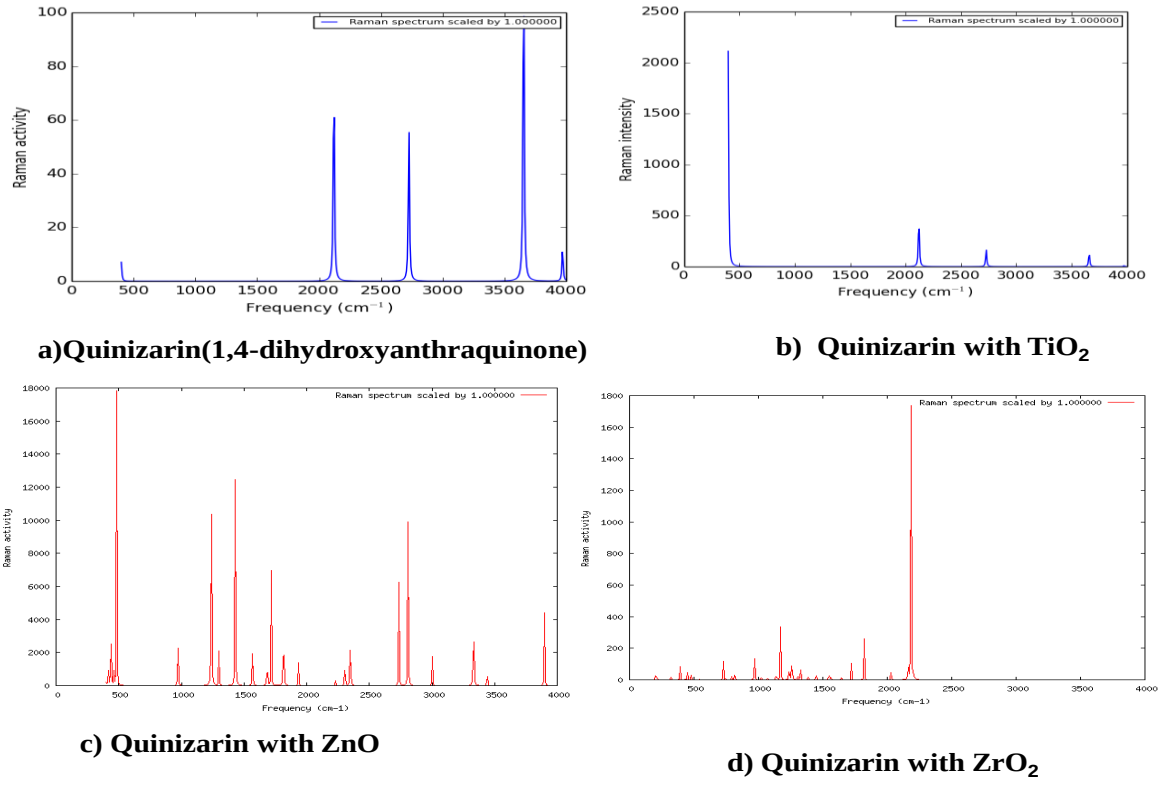

a)Quinizarin(1,4-dihydroxyanthraquinone)

b) Quinizarin with TiO_2

c) Quinizarin with ZnO

d) Quinizarin with ZrO_2

Figure 3 (a,b,c,d) Theoretical Analysis of FT-IR Spectrum of Quinizarin and Quinizarin/TiO_2 ,ZnO,ZrO_2

The theoretical results of FT-IR and FT-Raman spectra of quinizarin exhibit the characteristic bands at 968 , 1072, 1408, 1610 cm^{-1} are shown in Figure 2 (a,b,c,d). The calculated (scaled) wave numbers, observed IR, Raman bands, and assignments are given in Table 1. The methylene vibrations are expected in the regions 2900-3000 (stretching modes), 1100-1450 cm^{-1} (scissoring, wagging, and twisting modes) [19, 20]. The stretching modes of the CH_2 are assigned at 2849 and 2931 cm^{-1} theoretically and at 2931 cm^{-1} in the IR spectrum and 2961, 2935,2948,2916cm^{-1} in the Raman spectrum. The deformation modes of the CH_2group are assigned at 1342, 1302, 28 cm^{-1} theoretically. The rocking mode of the CH_2 group appears in the region 794 cm^{-1} for the quiizarin compound, the bands at 783 cm^{-1} in the IR spectrum and 782 cm-1 theoretically are assigned as a rocking mode.The asymmetric and symmetric stretching vibrations of the methyl group are expected in the regions 2948 and 2916 cm^{-1} and 2916-2978 cm^{-1} [20]. The asymmetric and symmetric deformations of the methyl group are expected in the regions 1308-1432 and 1342-1395 cm^{-1}[20]. The theoretical calculations give of CH_2 bending observed in 1426,1436,1448,1504 and 1460, 1440, and 1371 cm^{-1} as asymmetric and symmetric deformation bands and the corresponding bands observed in the IR spectrum and 1432,1448 the Raman spectrum. The C-C torsion generally appears in the regions 188,192,166 the wavenumber of which is coupled to the CC stretching vibrations [20], which occurs in the neighborhood of 900 $cm^{-1.}$ The bands at 1093 cm^{-1} in the IR spectrum, 951 cm^{-1} in the Raman spectrum, and 1092, 954 cm-1 (theoretical) were assigned as the rocking modes of the methyl group. The C=O stretching mode [19-21] is expected in the region 1937,1724,1817 cm^{-1} and in the present case, this mode appears at

1724 cm^{-1} in the IR spectrum and 1714 cm^{-1} in the Raman spectrum. The DFT calculations give this mode at 1687 cm^{-1}. The in-plane and out-of-plane C=H bending modes are expected in the regions 623,653cm1 respectively [20]. The C-O-C stretching vibrations are expected in the range of 1200-1100cm^{-1} (asymmetric) and 1050-950 cm-1 (symmetric) [20, 24].The skeletal C-O deformation can be found in the region 320±50 cm-1 [20]. In the present case, the band observed at c-c Torsion observed in 188,192,166, in IR 1013 cm-1 in the IR spectrum, 188,166 in the Raman spectrum. Joseph et al. [11] reported C-O-C stretching modes at 1221, 1219,991, 988 cm^{-1}cm-1 theoretically.C-C out of plane bending observed in 975,968,997 in the IR spectrum, 968,1042,10761072.Anthracene ring stretching modes are reported at1432, 1436,1439, 1448 in the IR spectrum, and 1438,1448, 1504 Raman spectrum by Wang et al.[28. Furthermore, anthracene ring stretching modes are reported in the range of 1262-1699 cm^{-1}cm-1 in the IR spectrum and at 1261-1636 cm^{-1} in the Raman spectrum and have been calculated to be in the range 1259-1622 cm-1 by Chandran et al. [10]. For the title compound, the anthracene ring stretching modes are observed at 1524, 1382, 1349, 1296, 1227, 1073, 986 cm^{-1}in the IR spectrum and at 1552, 1520, 1490, 1452, 1380, 1350, 1316, 1302, 1228, 1071, 985 c cm^{-1} in the Raman spectrum. These bands are assigned in the range 1600-982 cm^{-1} cm-1 theoretically. Most of these modes are not pure, but contain significant contributions from other modes, also. The other substituent sensitive deformation modes of the anthracene rings have also been identified and assigned. The in-plane CH deformation modes of the anthracene ring are observed at 1413, 1261,1164 cm-1 in the IR spectrum, and at 1417, 1260, 1160, 1139 cm-1 in the Raman spectrum. The corresponding theoretical values are in the range of 1123-1422 cm1. The out-of-plane modes of the anthracene ring are assigned at 968, 890, 706 cm-1 in the IR spectrum, at 975,794 cm-1 in the Raman spectrum, and in the range of 775-997 cm^{-1} theoretically. A strong band observed at 1290-1295 cm^{-1}assigned to C-OH bending modes. The observed bands at 1438 cm^{-1}nd 1340 $cm^{-1}$are assigned to C-H in-plane bending. The C-C stretching vibrations are assigned to the bands at 1232 $cm^{-1}$and 1216 cm^{-1}. The band found out at 517 cm^{-1} is assigned to C=C-C deformation vibrations. The torsion vibrations normally occur at 200 cm−1. The observed bands at 2950 cm−1, 2927 cm−1and 2977 cm−1are assigned to C-H stretching vibrations. The weak bands observed at 1643 cm−1and1515cm-1areassignedtoC=Cstretchingwhilethebandsat1380cm−1and1026cm−1are assigned to C-C stretching vibrations [16]. The characteristic peak observed at 493 cm−1becomes stronger, indicating the formation of the stretching mode of ZnO. This indicates the presence of ZnO nanoparticles is in calcined form. In FT-IR, the bands around 1636 cm−1and 3404 cm−1 correspond to the bending and stretching modes of the –OH groups present in the catalysts. The bands near 1043 cm−1and 487 cm−1are assigned to the bending vibration of Ti-O bonds. The characteristic band observed at 426 cm−1indicates the presence of ZrO2. The deposited thin films have facilitated the OH groups from Zr–OH and Ti–OH to form Zr-O and Ti-O interactions. The intensities of OH at 1635 cm−1,1516 cm−1and 1020 cm−1decreased while those of the stretching vibration of TiO2 and ZrO2 from 500 cm−1to 900 cm−1were comparatively increased. The observed bands at 576 cm−1 correspond to the zirconium vibration assignment. The observed broadness of the band

indicates that the ZrO2 powders are nanocrystals. The observed peaks at 1382 cm-1 and 1020 cm-1 related to the vibration mode of Ti –OH[8].

Quinzarin		**Quinzarin with TiO_2**		**Quinzarin with ZnO**		**Quinzarin with ZrO_2**		**Vibrational Assignment**
FTIR	**FT-RAMAN**	**FTIR**	**FT-RAMAN**	**FTIR**	**FT-RAMAN**	**FTIR**	**FT-RAMAN**	
	192			**188**	**188**	**166**	**166**	**C-C torsion**
	319		**319**	**319**	**319**			**CH_2 rocking**
					426	**426**		**Zro2**
358		**399**		**447**	**447**			**Zro2**
488				**465**	**465**	**486**	**486**	**Zro2**
				483	**486**	**486**	**486**	**Ti**
				493	**493**			**Zno**
	517					**501**	**501**	**C-C-C deformation**
	662			**629**	**629**	**623**	**623**	**=CH out of plane deformation**
	678					**653**	**653**	**=CH out of plane deformation**
706				**774**	**751**			
	775			**794**		**794**	**794**	**C-C Bending**
890								
968								
	997			**975**	**968**	**975**	**975**	**C-C In-of-Plane Bending**
	1026			**1021**	**1026**	**1020**	**1020**	**C-C Stretching**
				1043				**Tio2**
	1042					**1076**	**1076**	**C-C Out-of-Plane Bending**
1072								
	1120					**1141**	**1141**	**C-H Bending**
1160				**1158**				
	1211				**1229**	**1242**	**1248**	**CH_2 rocking**
1262	**1262**			**1242**	**1242**	**1261**	**1261**	**C-C Symmetric Stretching**

1308	**1309**					**1302**	**1302**	
1385	**1381**			**1302**	**1302**	**1384**	**1384**	**CH_3 Bending**
	1342					**1328**	**1328**	**CH_2 wagging**
				1382	**1382**			**Tio2**
1408								
						1432	**1432**	
	1426					**1448**	**1448**	**CH_2 Bending**
	1436			**1432**	**1432**			**CH_2 Bending**
	1439			**1448**	**1448**			**CH_2 bending**
				1504				
						1516	**1516**	**Zro2**
	1516			**1570**	**1570**	**1545**	**1545**	**C-C Stretching**
1603								
		163 5	**1635**	**1636**	**1636**	**1635**	**1635**	**Zr02**
	1642			**1645**	**1645**	**1645**	**1645**	**C=-H Asymmetric Stretching**
	1652			**1687**	**1687**	**1687**	**1687**	**C=-H Stretching**
1699								
1707								
	1739			**1719**	**1719**	**1724**	**1724**	**C=O Stretching**
				1751	**1787**			
						1817	**1817**	**C=O Stretching**
						1937	**1937**	**C=O Stretching**
				2161	**2183**			
2352	**2336**			**2231**	**2231**	**2231**	**2350**	**C-H Stretching**
	2849							**CH_2 symmetric stretching**
	2978							**C-H Stretching**
	2916							**CH_2 asymmetric stretching**
	2926							**C-H Asymmetric Stretching**
	2948							**CH_2 asymmetric stretching**
	3048			**3003**	**3003**			**=C-H stretching**
	3071							**=C-H stretching**
3455	**3423**			**3333**	**3333**			**O-H Symmetric Stretching**
3701								
	3803			**3898**	**3898**	**3333**	**3333**	**O-H Asymmetric Stretching**
						3441	**3441**	**O-H Asymmetric Stretching**
						3896	**3896**	**O-H Asymmetric Stretching**

						4604	**4604**	**O-H Asymmetric Stretching**

Table1 : 1 Theoretical spectrum of FTIR and FT-RAMAN assignments

Electronic Absorption Spectra and Sensitized Mechanism

Electronic absorption spectra of quinizarin and quinizarin with TiO2, ZnO, and ZrO2 in acetonitrile were obtained using TD-DFT- 6-311++G(d,p). The theoretical and the experimental results are reported in Figure 4 and 5 (a,b,c,d), respectively. It can be seen from the figures that the absorption in the visible region is much better than that in the UV region for quinizarin with TiO_2,ZnO, ZrO_2. The theoretical results show a significant red shift in the solvent than in a vacuum. This may be due to the smaller gap of materials which induces lower excited energies [17-19]. The result of optical absorption spectra shows that the film exhibit absorption intensity at 390 nm caused by ZnO semiconductor with electron transfer from the valence band to the conduction band. However, the absorption wavelengths above 586 nm correspond to visible n-π metal to ligand transfer occurs easily. The difference between optical absorption of the four kinds of wavelengths implies that an improvement in the degree of aggregation of nanocrystallites would induce more effective light scattering in the visible region. This would result in a decreased recombination rate to benefit the photocurrent density as well as the power conversion efficiencies. The redshift of absorption edges and narrowing of the band gaps, which are observed in the UV-Visible spectra, may improve the photovoltaic behavior of the synthesized hierarchical ZnO and ZnO with TiO_2. The TD –DFT calculations are capable of describing the spectral features of the dye sensitizers because of the agreement of line shape and relative strength as compared with the vacuum and solvent. This fact indicates that the solvent effects stabilize the frontier orbital of quinizarin with TiO_2, ZnO, and ZrO_2 as reported in Figure 5 (a,b,c,d). The absorption occurs in the visible and near-UV region, which is the most important region for photo-to-current conversion. Therefore, only the 10 lowest singlet/singlet transitions of the absorption band in the visible and near-UV region for quinizairin and the data calculated were based on the 6-311++G (d,p) results with solvent effect involved.

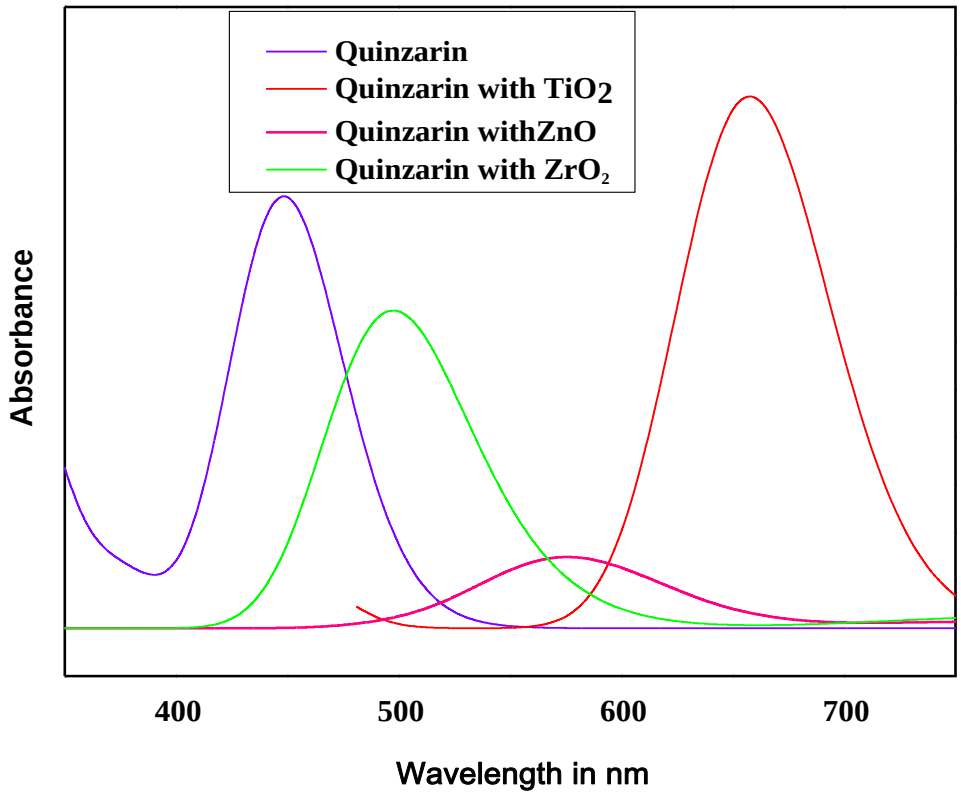

Figure 4 Theoretical absorption Spectrum of Quinizarin and Quinizarin/TiO_2 ZnO,ZrO_2

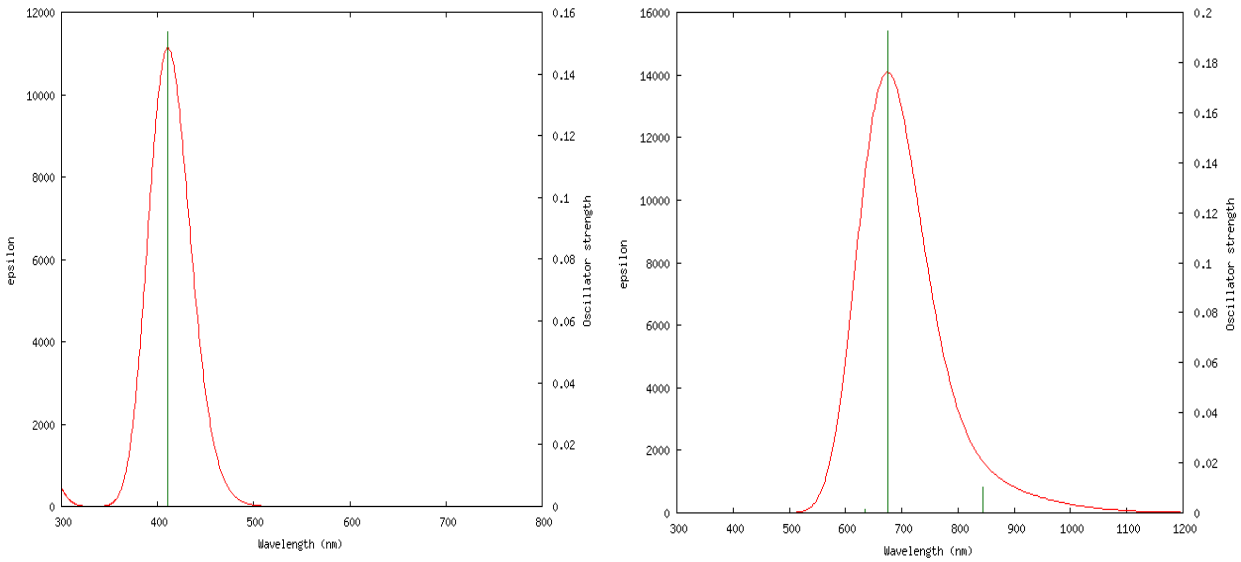

Figure 5 (a&b)The theoretical UV-Visible absorption Spectrm of Quinizairin and Quinizairin/TiO_2

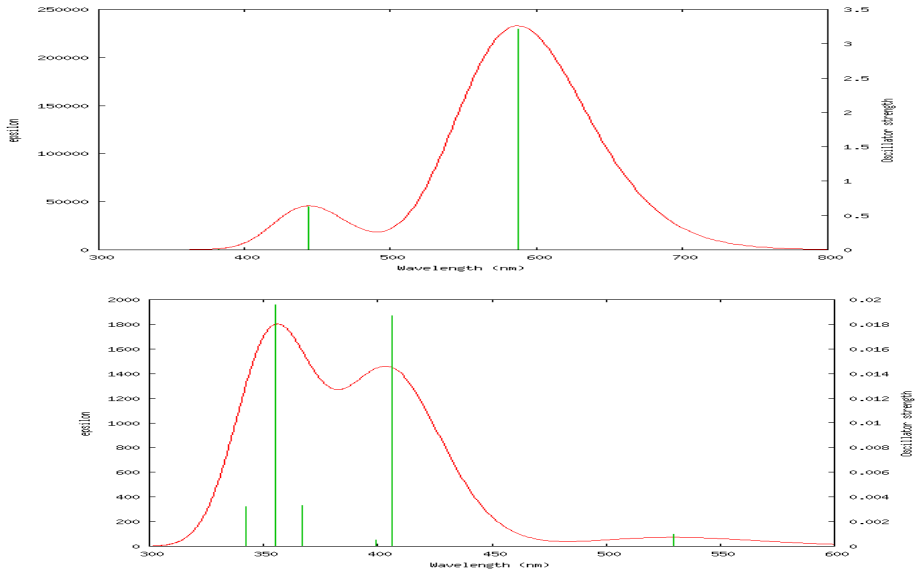

Figure 5 (c &d) The theoretical UV-Visible absorption Spectrm of Quinizairin /ZnO And Quinizairin/ZrO_2

Electronic absorption spectra of Quinizarin and in presence of TiO2, ZnO, ZrO2 in acetonitrile was performed using TD-DFT - 6-311++G(d,p) .calculations and experimental absorption spectrum are reported in Figure 4 and 5 (a,b,c, d). It can be seen from the Figure, the absorption in the visible region is much better than that in the UV region for Quinizarin with TiO_2 ZnO, ZrO_2 with experimental UV-Visible spectrum. The results of TD-DFT have an appreciable red-shift in the solvent, and the degree of red-shift in the solvent is more significant than that in a vacuum. The discrepancy between vacuum and solvent effects in TD-DFT calculations shows that a smaller gap of materials induces smaller excited energies [16,18].

The optical absorption spectra of films exhibit absorption intensity at 390 nm caused by ZnO semiconductor with electron transfer from the valence band to the conduction band. However, absorption wavelengths above 400 nm vary significantly revealing that the highest intensity 586 nm. This corresponds to visible n - π metal to ligand transfer that occurs easily. The difference between optical absorption of the four kinds of wavelengths implies that an improvement in the degree of aggregation of nanocrystallites would induce more effective light scattering in the visible region. This would result in a decreased recombination rate to benefit the photocurrent density as well as the power conversion efficiencies. The redshift of absorption edges and narrowing of the band gaps, which are observed in the UV-Visible spectra, may improve the photovoltaic behavior of the synthesized hierarchical ZnO and ZnO with TiO2.

The TD-DFT calculations are capable of describing the spectral features of the dye sensitizers because of the agreement of line shape and relative strength as compared with the vacuum and solvent. This fact indicates that the solvent effects stabilize the frontier orbital of Quinizarin with TiO2 is shown in Figure 5(a,b,c,d). It induces the smaller intensities and red-shift of the absorption as compared with that in a vacuum. To obtain the microscopic information about the electronic transitions, the

corresponding molecular orbital properties are checked. The absorption in the visible and near-UV region is the most important region for photo-to-current conversion.Therefore 10 lowest singlet/singlet transitions of the absorption band in the visible and near-UV region for quinizairin, and the data calculated were based on the 6-311++G (d,p) results with solvent effect involved.

HOMO – LUMO Analysis

The intramolecular charge transfer (ICT) from the electron-donating group to the electron-accepting group leads to electron injection from the donor (molecule ground state) to the acceptor state (semiconductor valence band) using energy less than bandgap value. The electron densities of the HOMO of quinizarin was localized on the donor and therefore the electron density of LUMO is especially localized on the bridge and acceptor units, therefore, the electronic transitions of quinizarin from HOMO to LUMO could lead on to intramolecular charge transfer from the donor units to the anchoring groups through the conjugated bridge. Therefore, when the dyes are anchored on the surface of TiO_2, ZnO, ZrO_2 and the LUMO centered on the anchoring moiety should enhance the orbital overlap with the titanium and subsequently favor the electron injection to the conduction band of TiO2ZnO and ZrO2. The difference of the energies of the HOMO and LUMO and therefore the bandgap is a measure of the excitability of the molecule and the isodensity plots of the frontier molecular orbital's energies of Quinizarin and Quinizarin / TiO2, Quinizarin / ZnO, Quinizarin/ ZrO2 is shown in Figure 6 (a,b,c,d) and this dye has good electron-separated states. While the calculated HOMO – LUMO bandgap energies of the quinizarin was found to be 2.82 EV and with TiO2was1.72 eV, with ZnO was 0.62eV and ZrO2 was0.52 eV respectively, leading to lowest transition was reduced, and this value is slightly smaller than the typical bandgap of quinizarin with metal oxides by experimental analysis was shown in Table 2. Furthermore, by taking under consideration of the cluster size effects and therefore the calculated HOMO, LUMO, HOMO– LUMO gap of the dye quinizarin with metal oxides [20], found in that the HOMO energies of this dye fall within the TiO2 gap. The above data also reveals that the interfacial electron transfer between semiconductor TiO2 electrodes and, therefore, the dye sensitizer quinizarin arein electron injection processes from excited dye to the semiconductor conduction band. This is often a sort of typical interfacial electron transfer reaction [21].

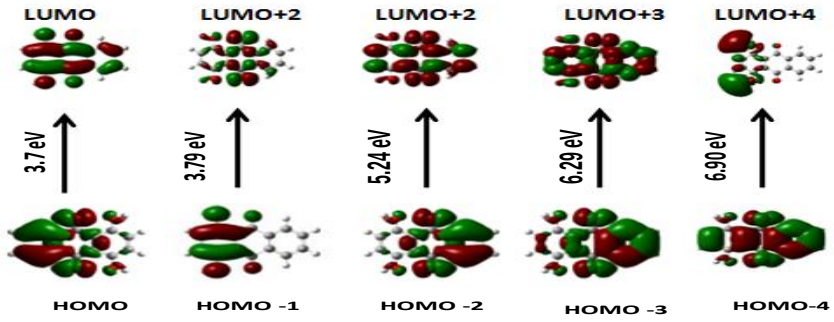

Figure 6 (a)Isodensity plots (isodensity contour = 0.02 a.u.) of the frontier orbitals of the dye with their corresponding orbital energies of Quinizarin

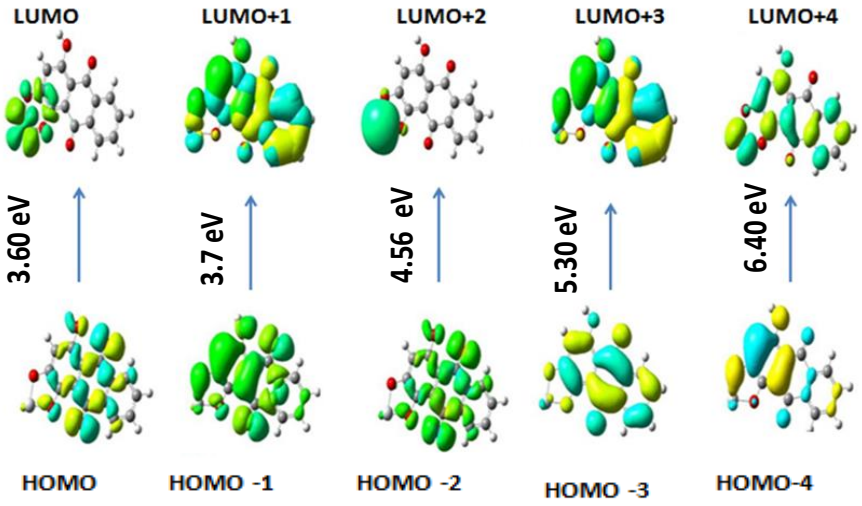

Figure 6 (b)Isodensity plots (isodensity contour = 0.02 a.u.) of the frontier orbitals of the dye with their corresponding orbital energies of Quinizarin/TiO_2

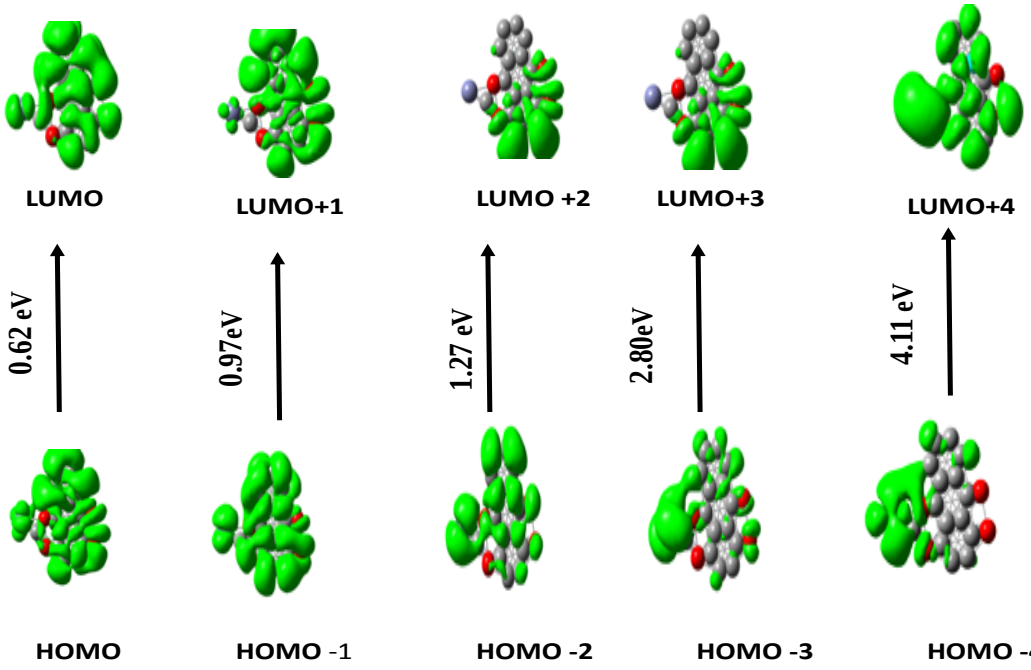

Figure 6 (c)Isodensity plots (isodensity contour = 0.02 a.u.) of the frontier orbitals of the dye with their corresponding orbital energies of Quinizarin/ZnO

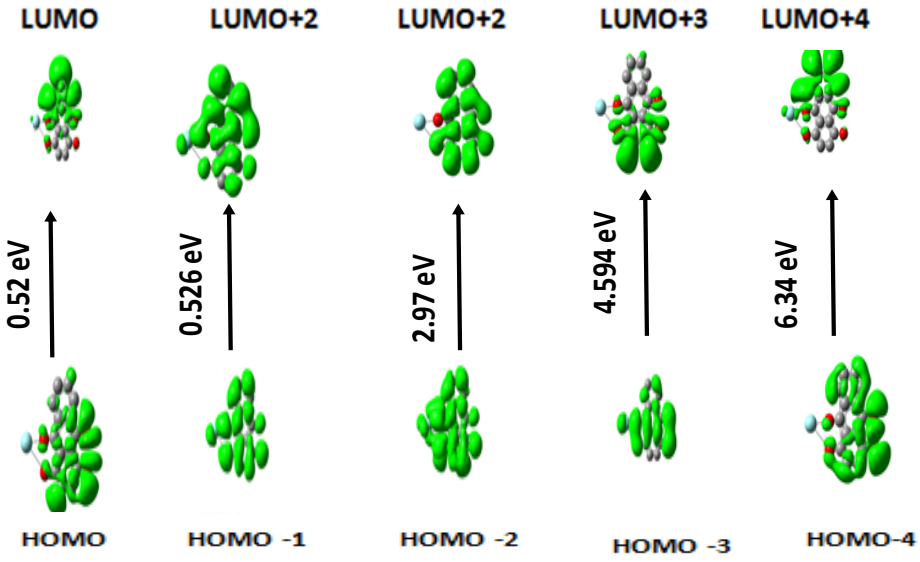

Figure 6 (d)Isodensity plots (isodensity contour = 0.02 a.u.) of the frontier orbitals of the dye with their corresponding orbital energies of Quinizarin/ZrO_2

The corresponding data of HOMO, LUMO, and HOMO-LUMO gaps and the isodensity plots of the frontier molecular orbital's energies of quinizarin and quinizarin / TiO2, quinizarin / ZnO, quinizarin / ZrO2 is shown in Figure 6 (a,b,c,d). The significant parameter like computed excitation energies, electronic transition configurations, and oscillator strengths (f) or the optical transitions with f > 0.1247 of the absorption bands in visible and near- UV-region for quinizarin for different metals have been reported in Table 3-6. The LUMO energy levels of the quinizarin dyes are much above that of TiO2ZnO and ZrO2 conduction band edge (-4.0 eV). Hence, the molecules in excited states of quinizarin have a robust capability to inject the electrons into TiO2, ZnO, and ZrO2 electrodes. The HOMO of the dye is less than that of I-/I-3 (-4.8 eV). Therefore, these molecules that lose electrons might be restored by getting electrons from the electrolyte. The order of the LUMO energy gap for quinizarin is low, thus the driving forces for electron injection from the molecular excitation state of the dyes to the TiO2 electrode. the HOMO-LUMO gap is 3.55 eV. The reduction in the bandgap, excites more electrons into the unoccupied molecular orbital. This maximizes the short current density and further enhances the conversion efficiency of the corresponding photovoltaic cell [22,23].

Table 2 :Band gap energy of Quinizarin and doped with TiO_2

Compound	**Energy gap in eV**	
	Experimental	**Theoretical**
Quinizarin	2.93 eV	2.82 eV
Quinizarin with TiO_2	2.3 eV	1.72 eV
Quinizarin with ZnO	3.1 eV	0.62 eV
Quinizarin with ZrO_2	2.95 eV	0.52 eV

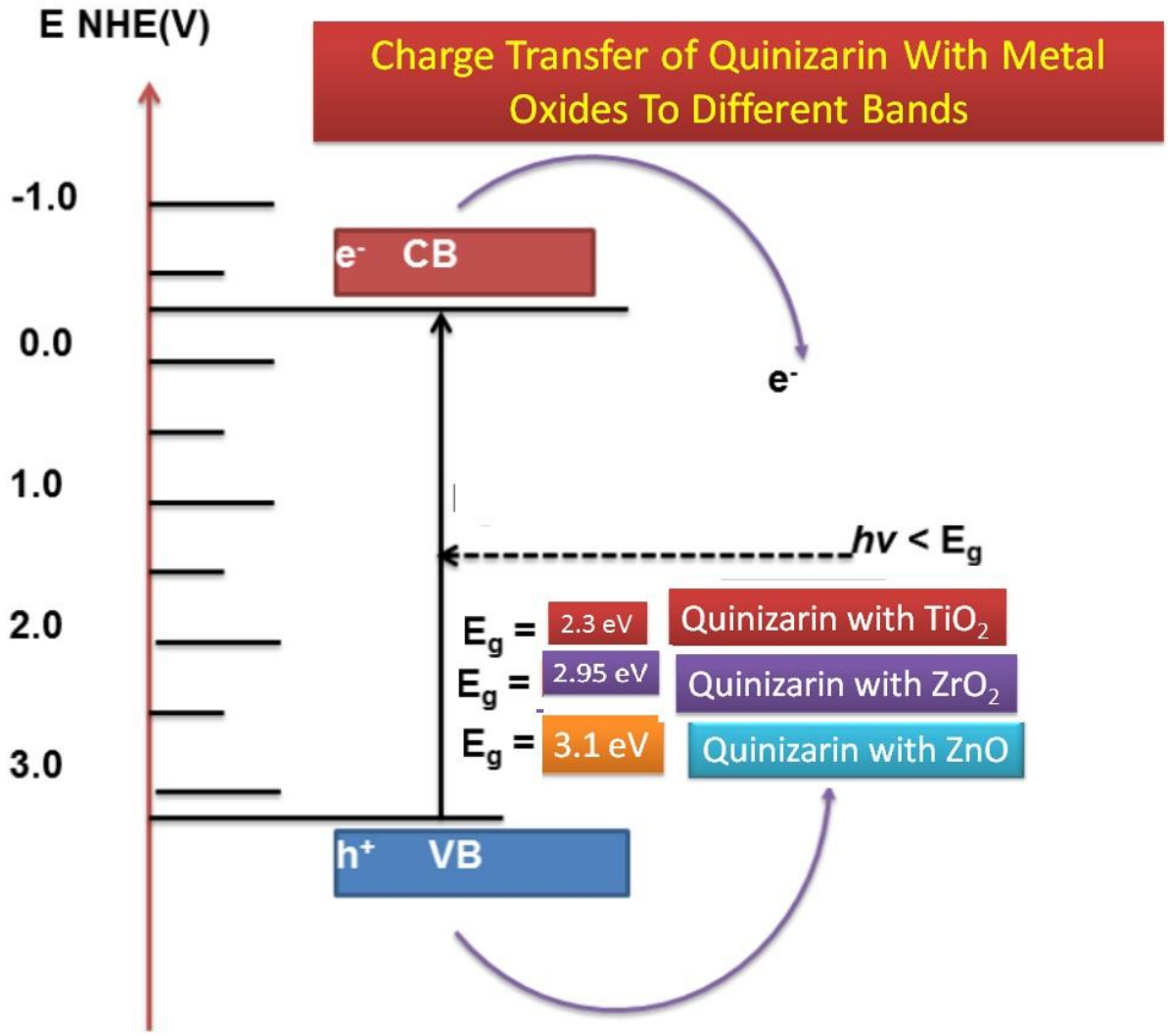

Figure 7 Schematic of diagram for Charge Transfer Of Quinizarin With Metal Oxides To Different Bandsgaps

Molecular Electrostatic potential (MEP)

MEP is widely used as a map representing the type of reactivity in a molecule.It displays the reactivity according to the colors of the region for electrophilic attack and the regions for nucleophilic attack.The MEPs of CPC and MAPC calculated at the B3LYP/6-311++G(d,p) method which are represented in Figure 5. Here different values of the electrostatic potential at the surface are represented by different colors. It increases in the order red > orange > yellow > green > blue. The negative (red color) regions of MEP were related to electrophilic reactivity (nucleophilic attack regions) and the positive (blue color) ones to nucleophilic reactivity (electrophilic attack regions). The MEP maps are in the ranges (-0.0682 (red) and 0.0681 (blue)) (-0.766 (red) and 0.0766 (blue)) for CPC and MAPC, respectively. The electron density map of MAPC has a larger range than that of CPC. This is due to the effect of different substitutions. MEP is connected to the ED and is a key in understanding sites for electrophilic and nucleophilic reactions along with hydrogen bonding interactions . The electrostatic potential V(r) is

ideal for analyzing processes based on the "structure" of one molecule by another, as in donor –substrate-acceptor interactions, because it is through their potentials that the molecular structures and bound metal oxides coupled with each other. To predict reactive sites of electrophilic and nucleophilic attacks for the investigated molecule, MEP at the B3LYP/6-31G(d,p) optimized geometry was calculated. The negative (red and yellow) regions of MEP were related to electrophilic reactivity and the positive (blue) regions to nucleophilic reactivity . From the MEP it is evident that the negative charge covers the C@O in the anthraquinone and aldehyde groups and the positive region is over the CAC bonds of the ring. The charge distribution was given in different color-coded electrostatic potential maps which permits the more direct comparison of surface charge distribution irregularities of test molecules and charge transfer was reported in Figures 7 and 8. It may be seen that the quinone moiety serves as a local acceptor, while the terminal rings are electron donors. In the case of quinizarin, the charge distribution of dyes, negative quinone moiety, and positive side rings of donors can be observed, which are associated with the strong electron-donating effect of quinolinic carbonyls. Directional charge location results in the formation of a significant dipole moment, which is 2.32 Debye for Ti, 1.19 Debye for ZnO, ZrO_2 for 4.08 Debye. The Mulliken charge distribution, in general, does not convey any significant modification between the studied scheme in the ground state, however, the Ti, Zn, Zr system shows the strongest intramolecular donor-acceptor character within the organic moiety. The negative charge is located at oxygen atoms and carbon atoms of the side rings, whereas the positive charge is located at the titanium atom and carbon atoms within carbonyl bridges. The results of the frontier orbital analysis show that the aromatic system is an electron donor, whereas the titanium center is an electron acceptor (Fig. 8). In our case, a competitive character of interaction occurs between titanium (IV) centers and anthraquinone dyes in terms of electron donor-acceptor interactions. The main transition for all modeled structures is the HOMO-LUMO transition within the significant contribution of higher excitations [24,25].

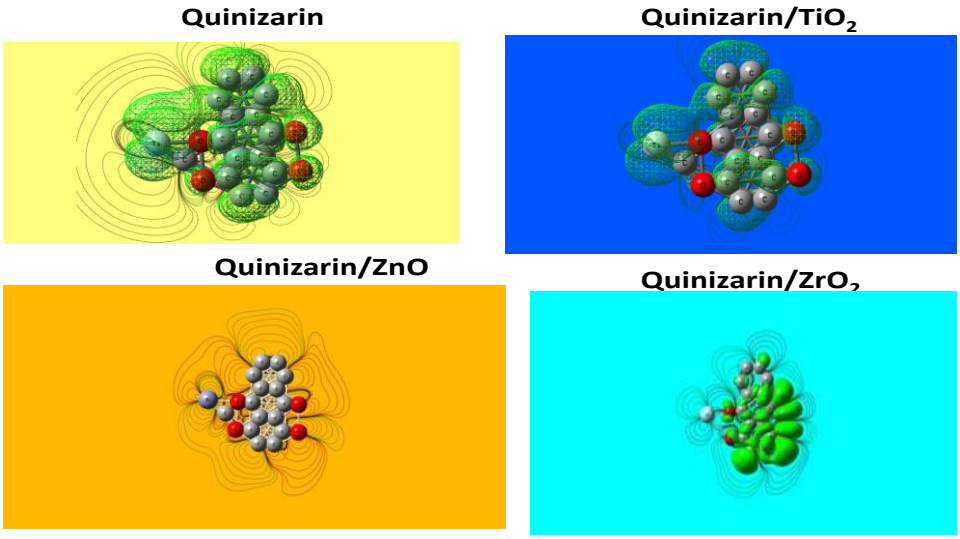

Figure 8 Schematic of diagram for electrostatic potential of Quinizarin With Metal Oxides

Table 3. Computed excitation energies, electronic transition configurations and oscillatorstrengths (f) or the optical transitions with f > 0.1247 of the absorption bands in visible and near- UV region for Quinizarin

No.	**Energy (cm-1)**	**Wavelength (nm)**	**Oscillator Strength**	**Major Contribution**
2	2.61	475	0.1740	H-1->LUMO (85%)
3	3.02	411	0.1536	H-2->LUMO (83%)
4	4.20	295	0.1330	HOMO->LUMO (82%)
5	4.31	288	0.0117	H-1->L+1 (89%)
6	4.44	279	0.0001	HOMO->L+1 (89%)
7	4.73	262	0.0012	H-2->L+1 (92%)
8	4.88	254	0.0875	H-4->LUMO (85%)
9	4.90	253	0.0004	H-5->LUMO (59%), HOMO->L+2 (-28%)
10	4.92	252	0.0057	H-5->LUMO (26%), HOMO->L+2 (54%)

Table 4. Computed excitation energies, electronic transition configurations and oscillatorstrengths (f) or the optical transitions with f > 0.1247 of the absorption bands in visible and near- UV region for Quinizarin with TiO_2

Energy (cm-1)	Wavelength (nm)	Oscillator Strength	Major Contribution
19191.29	521.0698	0	H-1->LUMO (95%)
20999.6	476.1996	0	H-2->LUMO (92%)
24935.61	401.0329	0.1482	HOMO->LUMO (98%)
33823.9	295.6489	0	H-1->L+1 (91%)
35453.15	282.0624	0.0138	HOMO->L+1 (92%)
35749.16	279.7269	0.0001	H-2->L+1 (94%)
38393.06	260.4637	0.0007	H-4->LUMO (93%)
39318.99	254.33	0.0582	H-5->LUMO (87%)
39519.02	253.0427	0.0017	H-1->L+2 (95%)
40011.83	249.9261	0.0307	HOMO->L+2 (91%)

Table 5. Computed excitation energies, electronic transition configurations and oscillatorstrengths (f) or the optical transitions with f > 0.1247 of the absorption bands in visible and near- UV region for Quinizarin with ZnO

.	Energy (cm-1)	Wavelength (nm)	Oscillator Strength	Major Contribution
2	1183.22352	8451.489	0.0014	HOMO->LUMO (204%)
3	4280.41392	2336.223	0.0013	HOMO->L+1 (99%)
4	6720.25792	1488.038	0	HOMO->L+2 (98%)
5	11015.99648	907.7708	0.0005	HOMO->L+4 (84%), HOMO->L+7 (11%)
6	12644.44112	790.8614	0.0033	HOMO->L+3 (104%)
7	13121.92464	762.0833	0	H-1->LUMO (98%)
8	16594.16544	602.6214	0.0002	H-1->L+1 (98%)
9	18613.79168	537.2361	0.011	HOMO->L+5 (91%)
10	19178.38368	521.4204	0.0007	HOMO->L+6 (94%)

Table 6 Computed excitation energies, electronic transition configurations and oscillatorstrengths (f) or the optical transitions with f > 0.1247 of the absorption bands in visible and near- UV region for Quinizarin with ZrO_2

No.	Energy (cm-1)	Wavelength (nm)	Oscillator Strength	Major Contribution
2	18882.38	529.5944	0.001	HOMO->LUMO (94%)
3	24612.98	406.2896	0.0187	H-1->LUMO (63%), HOMO->L+1 (21%)
4	25046.91	399.2508	0.0005	HOMO->L+1 (16%), HOMO->L+2 (75%)
5	27231.89	367.2166	0.0033	H-2->LUMO (73%), H-1->LUMO (10%)
6	28156.2	355.1615	0.0196	H-1->L+1 (38%), H-1->L+2 (15%), HOMO->L+1 (30%)
7	29199.89	342.467	0.0032	HOMO->L+3 (86%)

5. Conclusion

Dye-sensitized solar cells (DSSC) have attracted considerable interest over the last decades, as they offer the advantages of low fabrication cost, transparency and flexibility. In the present study, Quinizarin dye was investigated as to design and develop more efficient D-π-A dyes for the DSSC applications. The geometries, electronic structures, molecular analysis metal oxides/ Quinizarin were studied by using density functional

theory with hybrid functional basis set B3LYP-6-311G. The UV–Vis Spectra of the title compound was also investigated by using TD-DFT methods. The studies with anatase Quinizarin-TiO_2 sensitization imparted an enhancement in photo conductivity and broadening of photo action spectrum towards visible region. Based on the analysis of geometries, electronic structures and spectrum properties of Quinizarin-TiO_2, the role of quinone in 1,4 dihydroxy 9-10 anthroquinone is responsible to enlarge the distance between electron donor group and semiconductor surface resulting a decreased timescale of the electron injection rate. However, the recorded lower conversion efficiency of the reported dye indicates that the choice of the appropriate conjugate bridge in dye sensitizer is very important to improve and enhance the performance of DSSC.

References:

1. 1.O'Regan, B & Gratzel, M 1961, 'A low-cost, high-efficiency solar cell based on dye-sensitized colloidal TiO2 films', Nature, vol. 353, pp. 737-740.
2. W.R. Duncan, O.V. Prezhdo[2007], Theoretical studies of photoinduced electron transfer in dye-sensitized TiO2, Annu. Rev. Phys. Chem. 58 , 143.
3. M.K. Nazeeruddin, F. De Angelis, S. Fantacci, A. Selloni, G. Viscardi, P. Liska, S. Ito, B. Takeru, M. Gratzel (2005) Combined experimental and DFT-TDDFT computational study of photoelectrochemical cell ruthenium sensitizers, J. Am. Chem. Soc. 127, 16835-16847.
4. M.J. Lundqvist, M. Nilsing, P. Persson, S. Lunell (2006) DFT study of bare and dye-sensitized TiO2 clusters and nanocrystals, Int. J. Quantum Chem. 106, 3214-3234.
5. G. Calogero, J.-H. Yum, A. Sinopoli, G. Di Marco, M. Gratzel,and M. K. Nazeeruddin (2012), Anthocyanins and betalains as light-harvesting pigments for dye-sensitized solar cells, Solar Energy, vol. 86, no. 5, pp. 1563–1575.
6. J. Mech,a K. Mechb and K. Szaciłowski,TiO2–anthraquinone hybrids: from quantumchemical design to functional materials***Journal of Materials Chemistry C,*** 2015,3, 4148
7. A.S. *Polo*, M. K. Itokazu, and *N. Y. Murakami Iha (2006)*, Metal complex sensitizers in dye sensitized *solar cells*. *Solar Energy Materials* and *Solar Cells*, *vol. 90, no. 13, pp. 1936–1944.*
8. Marco Pagliai, Iacopo Osticioli, Austin Nevin, Salvatore Siano,Gianni Cardini, Vincenzo Schettino,**DFT calculations of the IR and Raman spectra ofanthraquinone dyes and lakes,** *Journal of Raman Spectroscopy*, 2018;1–16.
9. Mishra, M.K.R. Fischer, P. Bauerle, Metal-Free Organic Dyes for Dye-Sensitized Solar Cells: From Structure: Property Relationships to Design Rules, Angew. Chem. Int. Ed. 48 (2009) 2474-2499.A.
10. Mishra, M.K.R. Fischer, P. Bauerle, Angew. Chem. Int. Ed. 48 (2007) 2474.
11. Chaoyan Lia, Xichuan Yanga,_, Ruikui Chena, Jingxi Pana, Haining Tiana, Hongjun Zhub,Xiuna Wanga, Anders Hagfeldta,b, Licheng Suna,c, Anthraquinone dyes as

photosensitizers for dye-sensitized solar cells Solar Energy Materials & Solar Cells, 91 (2007) 1863–1871.

12. Justyna Mech , Maria A. Grela , Konrad Szaci1owski, Ground and excited state properties of alizarin and its isomers, Dyes and Pigments 103 (2014) 202-213.
13. Campbell, WM, Kenneth, W, Wagner, JP, Wagner, K, Walsh, RJ, Gordon, KC, Schmidt-Mende, L, Nazeeruddin, MK, Wang, Q, Grätzel, M & David, L 2007, 'Highly Efficient Porphyrin Sensitizers for Dye-Sensitized Solar Cells', Journal of Physical Chemistry C,
vol. 111, no. 32, pp. 11760-11762.
14. .Justyna Mech, Maria A Grela & Konrad Szaci1owski 2014, 'Ground and excited state properties of alizarin and its isomers', Dyes and Pigments, vol.103, pp. 202-213.
15. Theoretical Studies of Photoinduced Electron Transfer in Dye-Sensitized TiO2 7. Justyna Mech a,1, Maria A. Grela b, Konrad Szaci1owski a,c Ground and excited state properties of alizarin and its isomers,,Dyes and Pigments 103 (2014) 202-213
16. Eberle AR, Lerner MW. Separation and determination of scandium spectrophotometric
method using Alizarin red S. Anal Chem 1955;27(10):1551.
17. Crossley ML. Certain metallic derivatives of hydroxy-anthraquinones. J Am Chem Soc 1919;41:2083e90.
18. Di Iorio Y, Brusa MA, Feldhoff A, Grela MA. Electron transfer from photoexcited TiO2 to chelating alizarin molecules: reversible photochromic effect in Alizarin and TiO2 under UV irradiation. Chem Phys Chem 2009;10:1077-83.
19. T. ISHIWAKI¤, H. INOUE, A. MAKISHIMA, Electronic structures of Quinizarin complexed with TiO2 clusters,
20. JOURNAL OF MATERIALS SCIENCE 35 (2000) 1669 – 1674.
21. D. Jacquemin , V.Wathelet ,J. Preat , E.A.Perpete (2007), Ab initio tools for the accurate prediction of the visible spectra of anthraquinones,Spectrochim Acta A;67A:334–41 .

22. E. A. Perpete ,V. Wathelet ,J. Preat , C.Lambert , D.Jacquemine , E.A. Perpete , MolCULAR Physics, Comparison of theoretical approaches for predicting the UV/Vis spectra of anthraquinones, 105:325–31, 2007.
23. N. Belghiti, M. Bennani, M. Hamidi, S. M. Bouzzine and M. Bouachrine (2012), New compounds based on anthracene as a good candidate for organic dye-sensitized solar cells,Theoretical investigations , African Journal of Pure and Applied Chemistry, 6(14), pp. 164-72.

24. J. Mech,a K. Mechb and K. Szaciłowski,TiO2–anthraquinone hybrids: from quantumchemical design to functional materials,*J. Mater. Chem. C*, 2015, 3, 4148-4184
25. Ranjitha, S, Rajarajan, G, Gnanendra, TS, Anbarasan, PM & Aroulmoji, V 2015,'Optical Properties of Purpurin For Dye-Sensitized Solar Cells', Spectrochimica Acta Part A: Molecular and Biomolecular Spectroscopy, vol. 149, pp. 997-1008.

26. Ranjitha, S, Rajarajan, G, Aroulmoji, V & Anbarasan, PM 2014, 'Structural and Spectral Properties of 1,2-dihydroxy-9,10-anthraquinone Dye Sensitizer for Solar Cell Applications', Acta Physica Polonica A, vol. 135, no. 1, pp. 833-839.
27. M. Geetha a, P. Senthil Kumar a, K. Vasudevan a, A. Prakasam a, G. Meenakshi b, P.M. Anbarasan a, Molecular modeling of 3,4-pyridinedicarbonitrile dye sensitizer for solar cells using quantum chemical calculations, Journal of Saudi Chemical Society (2010) 14, 399–407
28. Mohr, T, Aroulmoji, V, Ravindran, RS, Müller, M, Ranjitha, S, Rajarajan, G & Anbarasan, PM ,2014, 'DFT and TD-DFT study on geometries, electronic structures and electronic absorption of some metal free dye sensitizers for dye sensitized solar cells', Spectrochimica Acta Part A: Molecular and Biomolecular Spectroscopy', vol.135, pp.1066-1073.